Original Paper

phys. stat. sol. (a) **204**, No. 6, 1645–1652 (2007) / **DOI** 10.1002/pssa.200675333

Ultra high sensitive detection of mechanical resonances of nanowires by field emission microscopy

S. Perisanu[1], **P. Vincent**[*, 1], **A. Ayari**[1], **M. Choueib**[1, 2], **D. Guillot**[1], **M. Bechelany**[2], **D. Cornu**[2], **P. Miele**[2], and **S. T. Purcell**[1]

[1] Laboratoire de Physique de la Matière Condensée et Nanostructures, Université Lyon 1, CNRS, UMR 5586, Domaine Scientifique de la Doua, 69622 Villeurbanne Cedex, France
[2] Laboratoire Multimatériaux et Interfaces, Université Lyon 1, CNRS, UMR 5615, Domaine Scientifique de la Doua, 69622 Villeurbanne Cedex, France

Received 13 October 2006, revised 30 January 2007, accepted 3 February 2007
Published online 23 May 2007

PACS 68.65.–k, 73.63.Fg, 79.70.+q

We present here highly sensitive measurements of nanowire mechanical resonances by analyzing Field Emission Microscopy (FEM) images from the nanowires while they are excited by sinusoidally time-varying voltages. Numerical analysis of the image blurring during frequency sweeps through resonances are shown to allow detection with $\simeq 100\times$ higher sensitivity as compared to our previous measurements where they were detected by the changes in the total field emission (FE) current. Furthermore since FEM approximately measures the end angle of the nanowire, this detection is more sensitive to higher resonance modes which in general have much smaller amplitudes. Observation of the mechanical response of SiC nanowires in FEM shows that they almost always present non linear mechanical behavior with large hysteresis and abrupt jump effects in their frequency response that are related to the large applied electric field. We approach the linear regime by reducing the excitation voltage and by using the sensitive image detection method.

1 Introduction

Nanostructures such as nanotubes and nanowires (NNs) are attracting great attention recently due to the promise of applications in sensing, materials reinforcement, vacuum microelectronics, and nanoelectromechanical systems (NEMS). The extremely small physical dimensions of these nanostructures imply high sensitivity to external perturbations. This characteristic has been recently investigated in the case of 100 nm thick cantilevers fabricated by ebeam lithography for zeptogram mass measurements [1] and biomolecule and gas sensing [2]. Measurements and understanding of the mechanical properties, excitation and response of pre-fabricated NNs, potentially even much smaller, are of prime importance for their successful bottom-up integration into NEMS.

Among the different techniques used to study the mechanical properties of these NNs, those that excite and detect their natural resonance frequencies are the most powerful because they measure both the Young's modulus and the quality factor as well as allowing to explore a rich space of linear, non-linear and high frequency response phenomena. The frequency response is obviously interesting for device and sensor applications. Such measurements have been performed in transmission electron microscopes

* Corresponding author: e-mail: pascal.vincent@lpmcn.univ-lyon1.fr, Phone: +33(0)472448548, Fax: +33(0)472432648

(TEM) [3] and scanning electron microscopes (SEM) [4, 5] where the natural resonances were excited by sinusoidally time-varying voltages and detected by the direct imaging. We have recently developed a variant of this method where the NN resonances are detected by monitoring the variation in field emission currents and patterns as a resonance is scanned in frequency [6].

The FE and electron microscopy configurations are complementary with different strengths and weaknesses which we are exploring by comparative studies in the FE and SEM environments. For examples, the microscopy allows a simpler interpretation of the resonances in parallel with determination of the NNs dimensions (see Fig. 1) while the FE is carried out in better vacuum, allows a wide selection of conditions such as varying temperature and gives a very direct differentiation of polarizations and mixed modes resonances. In this article we show how we can enormously increase the sensitivity for detecting resonances, or conversely lower the necessary excitation voltage, by numerically analyzing the FEM patterns. This is done during frequency scans by calculating the XY variance σ^2, which is equivalent to accurately measuring the 2D size of the image. This allows detecting resonances with $\simeq 100\times$ lower excitation voltages as compared to our previous measurements by the changes in the total FE current [6]. FEM is a direct observation of the nanowire's apex and relative changes in the near apex tilt angle. The later translates into a better sensitivity to higher order modes which have larger tilt angles near the apex and which are normally more difficult to excite and detect.

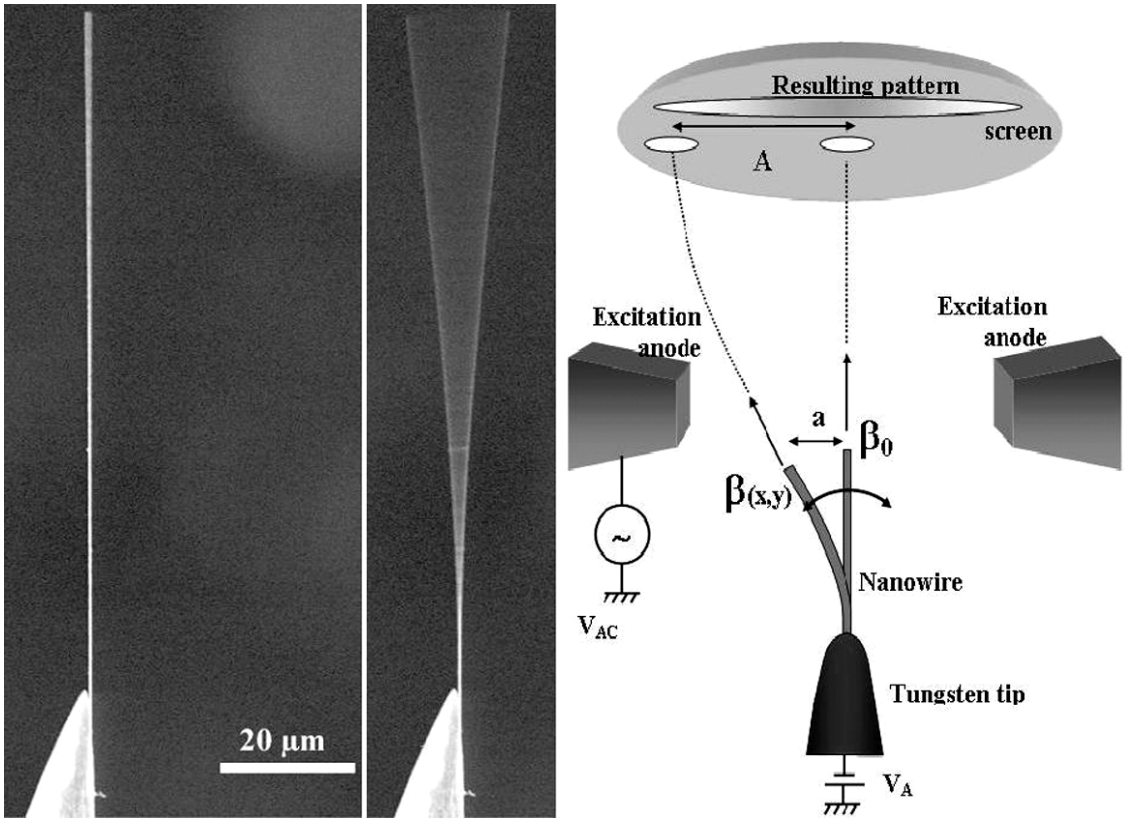

Fig. 1 (a) A SiC nanowire (99 μm length, 173 nm radius) similar to the one used in the experiment mounted on a tungsten tip. Left: at rest; right: vibrating in its fundamental mode. The nanowires are covered with a very thin layer ($\simeq 1$ nm) of graphite that makes them conducting. (b) Schematic of the Field Emission setup. The excitation amplitude V_{AC} is mV to Volts and the extraction voltage V_A is $300-600$ Volts.

2 Experimental

The samples studied here were mono-crystalline SiC nanowires covered by nm-thick turbostratic amorphous carbon layers (denoted SiC@C; sometimes termed nanocable). Recently a breakthrough in the mass production of SiC-based nanowires was achieved with the discovery of a commercially competitive process allowing fabrication of large amounts of SiC-based nanowires with tunable geometric features and possible in-situ chemical-surface modification [7]. According to this technique, SiC@C nanocables are produced by the high-temperature reaction of carbon-based volatiles, generated in-situ by the thermal decomposition of polypropylene, with SiO(g) at the lower face of a graphite condensation plate. The as-obtained 1D nanostructures were characterized as having cubic-SiC cores of 20–300 nm diameter covered by turbostratic carbon layers with controllable thicknesses of 1–40 nm, forming SiC@C nanocables. Detailed experimental procedure and complete characterization of these SiC@C nanocables have been reported elsewhere [7, 8].

These nanowires were glued using micro manipulators to the apexes of etched tungsten tips. The nanowires are straight and approximatively aligned along the tip axis. An example SEM image is shown in Fig. 1 where we have added an image of the nanowire resonating in its fundamental mode for illustrative purposes. For these FE studies we used a SiC wire of 284 nm diameter and 128 μm length. The tungsten tip/nanowire was mounted on a heating loop which was then inserted into a classical field emission configuration in ultrahigh vacuum (10^{-10} Torr).

As schematized in Fig. 1, the tip/nanowire is mounted in a triode configuration with an intermediary quadrupole extraction anode at a distance of $\simeq 2$ mm. A high enough voltage V_A is applied to the tip such that electrons are field emitted from the nanowire apex. The electrons accelerate away from the apex, pass through the quadrupole and impinge on a phosphor screen placed at about 3 cm in front of the tip. A field emission pattern appears on the screen (Figs. 1, 2) which is recorded by a digital video camera simultaneous to emission current measurements with a sensitive electrometer. In these experiments V_A was varied from –300 to –600 V for electron emission.

An additional AC excitation voltage V_{AC} is applied to the anodes. V_A and V_{AC} induce an electrical charge mostly at the end of the nanowire and the corresponding electrical force excites the mechanical oscillations when the frequency of the excitation voltage corresponds to a mechanical resonance frequency of the nanowire. A modification of the emission current and the shape of pattern is then ob-

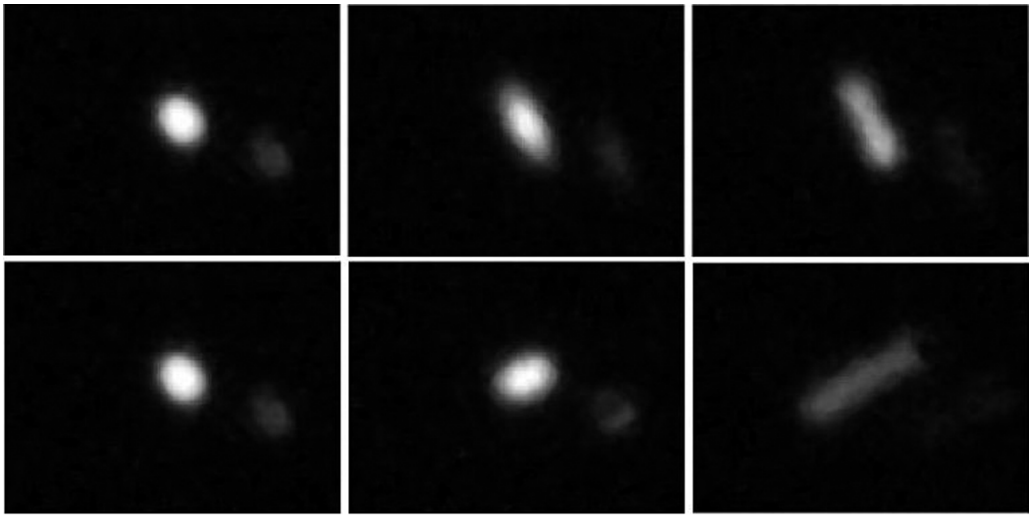

Fig. 2 Field emission patterns at slightly different frequencies for two perpendicular polarizations. Left to right increasing frequency. Bottom sequence near 32965 Hz, top sequence near 33045 Hz.

served. The resonance frequencies depend strongly on the dimensions for the different N & Ns studied (see below) and varied from 5 kHz to 20 MHz in our experiments. Both the emission current and the computer-processed video images are used to extract the relative oscillation amplitude. Since our camera is limited at 25 Hz, and our electrometer to 3 Hz, we only detect the time-averaged emission pattern and current.

The type of images we measure are illustrated in Fig. 2 which shows two sequences of FEM images near two mechanical resonances closely spaced in frequency. The patterns widen as the resonance maximum is approached and the vibration amplitude increases. In general we find vibrations with two nearby orthogonal polarizations (see below).

3 The image analysis method

The emitted current varies as the resonance is scanned because of the variation of the position of the nanowire apex and hence the field amplification factor. As the current varies exponentially in field at the emission zone, small variations of the field amplification factor β can produce large variations of the measured current. However the dependance of the field on the amplitude of oscillation is a second order effect (we are at an extremum) and as well in our present setup the measured current is averaged over the oscillation. These together mean that the total current measurement does not allow us to detect very small vibrations. For this reason we have turned to the analysis of the FEM images which improves enormously our signal to noise ratio.

To understand the image analysis method let us first start with a quick mathematical description of the vibrating rigid beam. An important aspect is that, as we showed previously, the resonance frequencies increase linearly and by a significant amount (up to 10×) as a function of V_A [6]. This is because the large applied electric field at the apex for FEM induces a stress T along the wire, proportional to V_A^2. The equation of motion for this singly-clamped, rigid and end-stressed beam is:

$$-EI\frac{\partial^4 u}{\partial z^4}+T\frac{\partial^2 u}{\partial z^2}=\rho S\left[\frac{\partial^2 u}{\partial t^2}+\gamma\frac{\partial u}{\partial t}\right], \tag{1}$$

where z is the position along the wire, u the displacement, γ the dumping coefficient, E the Young modulus, ρ the density, $S=\pi r^2$ the cross section, r the radius and $I=\pi r^4/4$ the geometric moment.

The solution of this equation consists of a sequence of eigenfunctions [9] with frequencies increasing with the applied voltage (or electric field). In the limit of the large fields necessary for FE, we have a tunable oscillator with a linear dependence of the frequency on the applied voltage, as confirmed by the experiment [6].

To understand how the image is related to the oscillation amplitude consider the trajectories of the emitted electrons. The electric field surrounding the end of the wire is strongly enhanced by the tip effect and the near apex equipotential lines have a hemispherical shape. The electron beam is radially accelerated in the neighborhood of the wire apex and only weakly deflected afterwards, as shown in Fig. 1. Thus to a first approximation the amplitude of the pattern oscillation A on the screen is proportional to the angle at the end of the wire. Furthermore for a given oscillation mode, the ratio between the angle and the displacement at the end of the wire a is constant, and therefore $A = M \cdot a$ where M is a magnification factor that increases with increasing oscillation mode number. This last fact makes this technique particularly interesting for studying higher modes.

The shape of the time-averaged oscillation pattern (or the light intensity distribution) $I_{osc}(x,y)$ is given by:

$$I_{osc}(x,y)=I_0(x,y)\cdot P(x,y)\ , \tag{2}$$

where $I_0(x,y)$ is the pattern when the wire is at rest, $P(x, y)$ the probability density of finding the oscillator at the position (x, y) and "$*$" the convolution product symbol. For a harmonic oscillator with an am-

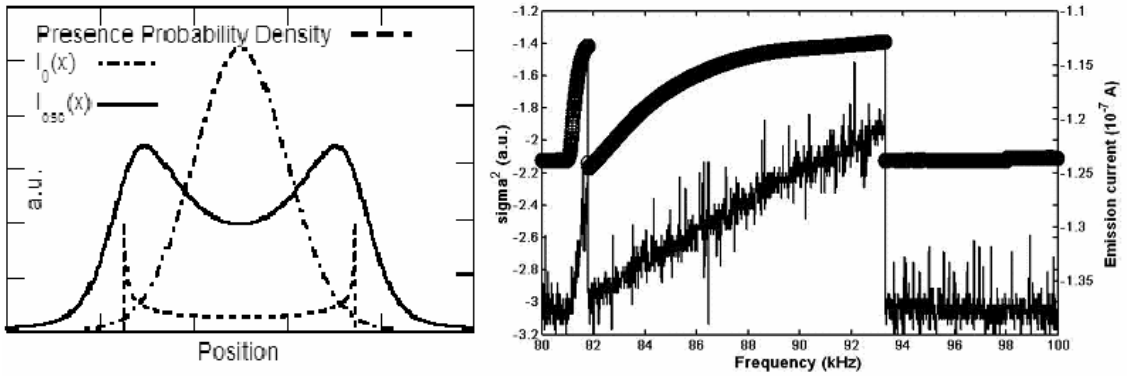

Fig. 3 Left: Presence probability density of a harmonic oscillator $P'(x) = \int_{-\infty}^{\infty} P(x,y)\,\mathrm{d}y$ as given by Eq. (3), a Gaussian intensity profile $I_0(x)$ and their convolution to give $I_{\mathrm{osc}}(x)$. One can compare to Fig. 2 to see that $I_0(x)$ and $I_{\mathrm{osc}}(x)$ correspond well to the non-oscillating and oscillating light distribution patterns. Right: Field emission current (–) and σ^2 (∘) response during an "up" frequency sweep through the resonance. The wire is the one in Fig. 1 and the excitation voltage was 1 Volt. The two response functions are perfectly matched in the frequency scale and the signal to noise ratio is about 100 times better for the image analysis method.

plitude A along the x direction,

$$P(x,y) = \frac{\delta(y)}{\pi\sqrt{A^2 - x^2}} \tag{3}$$

inside the interval $-A < x < A$ and 0 outside, with $\delta(y)$ the Dirac distribution. The form of the 1D probability density and its convolution with a Gaussian intensity profile is shown in Fig. 3. It resembles a line scan across the SEM image of the vibrating nanowire shown in Fig. 1 and the FEM images shown in Fig. 2. The peaks at the image extremities just reflect the fact that the oscillator spends more time at the maximum amplitude points where its velocity is lowest.

The easiest way to determine the amplitude of the oscillation is to use the variance of the light intensity distribution. For the x direction and a distribution $I(x, y)$, the variance σ_x^2 is defined as:

$$\sigma_x^2 = \frac{\int_{-\infty}^{\infty} x^2 I(x,y)\,\mathrm{d}x\,\mathrm{d}y}{\int_{-\infty}^{\infty} I(x,y)\,\mathrm{d}x\,\mathrm{d}y} - \left[\frac{\int_{-\infty}^{\infty} xI(x,y)\,\mathrm{d}x\,\mathrm{d}y}{\int_{-\infty}^{\infty} I(x,y)\,\mathrm{d}x\,\mathrm{d}y}\right]^2 \tag{4}$$

and in an analogous way for the y direction. The total variance is given by $\sigma^2 = \sigma_x^2 + \sigma_y^2$. Using Eqs. (2)–(4) it is easy to prove that the variance of the oscillating distribution σ_{osc}^2 is related to the variance of the distribution at rest σ_0^2 by:

$$\sigma_{\mathrm{osc}}^2 = \sigma_0^2 + \frac{A^2}{2}. \tag{5}$$

Therefore in Eq. (5), σ_{osc}^2 as a function of the frequency is the square of the response curve of our system to an additive constant.

Our video camera captures images with 625×480 pixels 8 bit encoded which translates into about 100 pixels/cm. The emission pattern is typically 1 cm so $\simeq 100 \times 100$ pixels. The integrals in Eq. (4) are

transformed into sums on an interesting region around the pattern. The choice of this zone is a compromise between the noise level (the noise contribution increases with the distance to the center of the emission pattern) and the intensity of the emission pattern outside this region.

How does noise coming from light intensity not generated by the nanowire's emission pattern affect this method? It is easy to prove that the effect of a noise, $I_n(x, y)$, is a multiplicative constant C before the $A^2/2$ term in Eq. (5), with:

$$C = \frac{\int_{-\infty}^{\infty} I_0(x,y)\,\mathrm{d}x\,\mathrm{d}y}{\int_{-\infty}^{\infty} (I_0(x,y)+I_n(x,y))\,\mathrm{d}x\,\mathrm{d}y}. \tag{6}$$

The effect of background light is negligible for our measurements because the nanowire is the only emitter and because the image is intense and carried out in a dark room. The real noise that is seen in the experimental curves comes from the instability in the emission current, setting a lower limit to the measured amplitude at 2 pixels. Such extremely low amplitude measurements can be achieved only by averaging the light distribution of the emission pattern. The total time of measurement is limited by the stability of the oscillator to about one hour after which thermal treatment must be made in order to clean the nanowire. This limits the number of measurements to be averaged, especially for the lower modes for which the mechanical relaxation time is not negligible. The gain in signal to noise ratio of the image method as opposed to the total emission current is demonstrated in Fig. 3 to be $\simeq 100$. In fact this has allowed us to observe and identify up to six of the harmonic resonances predicted by linear response theory. To our knowledge it is the first measurement in the literature beyond the 4th mode.

Another strong feature of these measurements is that response functions are not simple Lorentzians but display the characteristic Duffing mode behavior of non-linear driven systems [10] (see below). The very straight form of the total current response curve is a sign of a very high degree of non-linear response. In that case the curve from the image analysis bends over towards high frequency because part of the FE pattern extended outside of the screen at the largest oscillation amplitude.

We have noted that in general the resonances are split in a pair of two polarizations closely-spaced in frequency. For a perfectly cylindrical and crystalline wire, perfectly positioned on the support tip, the oscillation frequency in any direction perpendicular to it's axis should be the same. However in our case the nanowires have an angle with respect to the tip and small defects which alter the rotational symmetry and give them two eigendirections of oscillation with slightly different frequencies. The numerical image treatment allows us to determine the angle α of the eigendirections with respect to a given direction x:

$$\tan\alpha = \sqrt{\frac{\sigma_{\mathrm{osc},y}^2 - \sigma_{0,y}^2}{\sigma_{\mathrm{osc},x}^2 - \sigma_{0,x}^2}}. \tag{7}$$

In Fig. (4) we show the analysis for a pair of resonances with the eigendirections Ox (left upper graph) and Oy (left lower graph). Note that the component of σ perpendicular to the polarization direction cannot be distinguished from the noise which means that we can selectively measure one resonance at a time. This may be useful when the response functions overlap.

In general the response curves for the nanowires we studied in FE show jumps (see Fig. 3) and hysteresis which is a signature of non-linear behavior. Figure 4 shows the frequency response of the nanowire for an excitation $V = 20$ mV. The hysteresis and jumps decrease when the excitation amplitude is diminished (Fig. 4), and the linear regime is approached only for very low excitation. Non-linear effects are caused by the variation of the stress T and of the excitation force with the position of the wire and will be explored for our FE configuration in a future publication. These effects widen the response curves and thus mask the measurement of the Q-factor which is a further reason to use the image technique to measure very small vibrations. By using this technique in conjunction with averaging over 64 sweeps we reached a linear response with 1 mV excitation with Q-factor 159 000 [11].

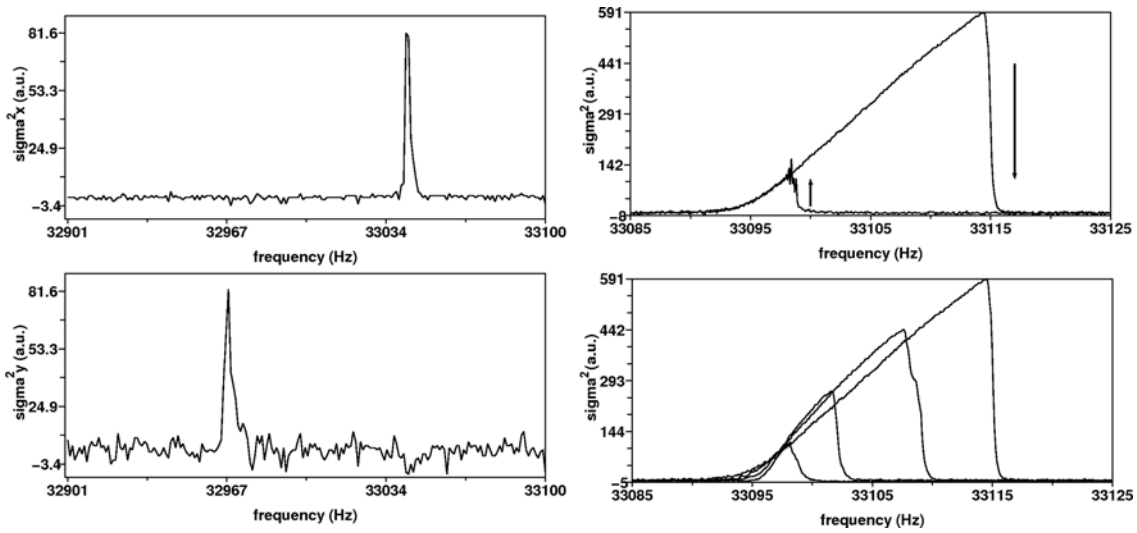

Fig. 4 Left: σ_x^2 (top) and σ_y^2 (bottom) as a function of frequency for *Ox* and *Oy* polarizations. For this experiment the eigendirections of the nanowire corresponded exactly to the *Ox* and *Oy* axes. Right, top: Square amplitude as a function of the frequency for an excitation of 20 mV showing hysteresis between the "up" and "down" frequency sweeps. Right, bottom: Square amplitude as a function of the frequency for excitations of 2, 5, 10 and 20 mV, for "up" frequency sweep. For a 2 mV excitation the response curve is almost linear.

4 Discussion

It is interesting to quantify what we mean by highly sensitive detection with respect to nanowire end angle and movement and make predictions for any NN. To calculate this we need the corresponding geometrical formulas and several physical constants. From geometrical considerations the minimum NN apex angle displacement $\Delta\theta$ in terms of the minimum detectable amplitude in pixels, p, the number of pixels/cm in the image, m, and the distance NN-screen, L is:

$$\Delta\theta = \frac{p}{m \cdot L} = 0.4^\circ \,. \tag{8}$$

Converting this to apex displacement is done by using the solution of Eq. (1). The higher the mode, the higher the ratio of angle to displacement and hence the better the sensitivity of the method to measure oscillations. In Table 1 are listed the minimum detectable displacement for our nanowire for different modes. We have used $E = 530$ GPa measured on another nanowire of the same type by induced vibrations in the SEM, $\rho = 3200$ kg/m^3, $L = 3$ cm, $d = 250$ nm and $l = 128$ μm. A magnification of several hundred to several thousands and minimum amplitude detection (min amp) down to 50 nm are predicted.

Table 1 Magnification and minimum detectable amplitude as a function of the oscillation mode.

mode	magnification	min amp (nm)
1	306	656
2	1098	182
3	1825	110
4	2567	78
5	3305	61
6	4043	49

For the first mode the minimum amplitude already corresponds to only 2–3 times the wires's diameter. Our experience is that this is difficult to observe using electron microscopy because while zooming to obtain such a magnification, the electron beam influences the wire's movement and also degrades the nanowire. For the progressively higher modes it will become even more difficult or even impossible for electron microscopy to image such low amplitude oscillations.

The values of Table 1 scale roughly inversely with nanowire length. Projecting this to a single wall nanotube (SWNT) with diameter 1.4 nm and length 0.5 μm gives a minimum detection of 5 nm for the first mode.

5 Conclusion

We have presented a new highly sensitive technique of detection of mechanical resonances for nanowires and nanotubes. The technique of resonance detection by FE presented here is an alternative to the microscopy measurements as well as optical [12–14], capacitive [15, 16] or electromagnetical [17, 18] techniques. The main advantages of this high sensitivity technique are the increasing sensitivity to higher modes, the easy distinction of different polarizations simultaneous to a determination of the Q factor and that it does not require sophisticated detection electronics. This has allowed us to detect and to study up to 6 harmonic modes of vibration for our nanowire and to enter into the linear regime of vibrations despite the strong non-linear effects that are associated with the large electric field. This technique may be useful in field emission vacuum nanoelectronics devices where the use of spilt detection anodes would be somewhat similar to our image analysis technique [19].

Acknowledgements This research has been carried out within the "Lyon Nanotube and Nanowire Working Group". May Choueib thanks the Lebanese CNRS for the financial support.

References

[1] Y. T. Yang, C. Callegari, X. L. Feng, K. L. Ekinci, and M. L. Roukes, Nano Lett. **6**, 583 (2006).
[2] C. P. Green and J. E. Sader, J. Appl. Phys. **98**, 114913 (2005).
[3] P. Poncharal, Z. L. Wang, D. Ugarte, and W. A. de Heer, Science **283**, 1513 (1999).
[4] M. F. Yu, G. J. Wagner, R. S. Ruoff, and M. J. Dyer, Phys. Rev. B **66**, 073406 (2002).
[5] D. A. Dixin, X. Chen, W. Ding, G. Wagner, and R. S. Ruoff, J. Appl. Phys. **93**, 226 (2003).
[6] S. T. Purcell, P. Vincent, C. Journet, and V. T. Binh, Phys. Rev. Lett. **89**, 276103 (2002).
[7] M. Bechelany, D. Cornu, and P. Miele, Patent No. WO 2006/067308 (06/29/2006).
[8] M. Bechelany, D. Cornu, F. Chassagneux, S. Bernard, and P. Miele, J. Opt. Adv. Mater. **8**, 638 (2006).
[9] C. Vallette, Mecanique de la corde vibrante (Hermes, Paris, 1993).
[10] See for example: Ali H. Nayfeh and Dean T. Mook, Non-linear oscillations (Wiley-VCH, Weinheim, 2004).
[11] S. Perisanu, P. Vincent, A. Ayari, M. Choueib, D. Guillot, M. Bechelany, D. Cornu, and S. T. Purcell, Appl. Phys. Lett. **90**, 043113 (2007).
[12] D. W. Carr, S. Evoy, L. Sekaric, H. G. Craighead, and J. M. Parpia, Appl. Phys. Lett. **75**, 920 (1999).
[13] J. Yang, T. Ono, and M. Esashi, Appl. Phys. Lett. **77**, 3860 (2000).
[14] G. M. Kim, S. Kawai, M. Nagashio, H. Kawakatsu, and J. Brugger, J. Vac. Sci. Technol. B **22**, 1658 (2004).
[15] M. D. LaHaye, O. Buu, B. Camarota, and K. C. Schwab, Science **304**, 74 (2004).
[16] K. Schwab, Appl. Phys. Lett. **80**, 1276 (2002).
[17] A. B. Hutchinson, P. A. Truitt, K. C. Schwab, L. Sekaric, J. M. Parpia, H. G. Craighead, and J. E. Butler, Appl. Phys. Lett. **84**, 972 (2004).
[18] A. N. Cleland and M. L. Roukes, Appl. Phys. Lett. **69**, 2653 (1996).
[19] M. I. Marques, P. A. Serena, D. Nicolaescu, and A. Correia, J. Vac. Sci. Technol. B **18**, 1068 (2000).

